Available online at www.sciencedirect.com
SCIENCE DIRECT
Journal of Catalysis 234 (2005) 182–190
JOURNAL OF CATALYSIS
www.elsevier.com/locate/jcat

Structure and catalytic properties of nanostructured molybdenum sulfides

G.A. Camacho-Bragado [a,*], J.L. Elechiguerra [a], A. Olivas [b], S. Fuentes [b], D. Galvan [b], M. Jose Yacaman [a,*]

[a] *Department of Chemical Engineering and Texas Materials Institute, University of Texas at Austin, Austin, TX 78712, USA*
[b] *Centro de Ciencias de la Materia Condensada - UNAM, Ensenada, B.C. CP 22800, Mexico, Mexico*

Received 28 March 2005; revised 26 May 2005; accepted 9 June 2005

Available online 19 July 2005

Abstract

A nanostructured form of molybdenum disulfide/dioxide was prepared by a two-step hydrothermal/gas phase reaction. The material was composed of a solid MoO_2 core with MoS_{2+x} crystallites nucleating on its surface. Most of the MoS_{2+x} consisted of nanowires, which are 14 to 30 nm long and are about one MoS_2 unit cell wide. High-resolution electron microscopy (HREM), electron diffraction, energy-dispersive X-ray spectroscopy (EDS), high-angle annular dark-field (HAADF) and X-ray diffraction were used to characterize the structure of the catalysts. The morphology does not depend strongly on the parent oxide, since both samples presented the oxide and sulfide phases; however, the abundance of nanowires depends on the thickness of the original oxide crystal. The catalytic activity and selectivity measurements of the resulting unsupported catalysts are also presented. In both samples, a higher selectivity for hydrogenation over sulfur removal was found.

Keywords: HREM; Molybdenum sulfide nanowires; Hydrotreating catalyst

1. Introduction

Molybdenum and other transition-metal sulfide-based (TMS) hydrotreating catalysts were developed early in the twentieth century [1,2] and soon became extensively used in refineries worldwide, since they present activity towards hydrogenation and sulfur removal. Their tolerance for sulfur represented a great advantage over noble metal catalysts, which are easily poisoned by even small amounts of sulfur.

The need to develop better fuels and, as a consequence, better hydrodesulfurization catalysts (HDS) is based on three main facts:

(i) The more stringent regulations starting in 2006 will require maximum sulfur levels of 15 ppmw in diesel, 30 ppmw in gasoline, and 3000 ppmw in jet fuel [3];
(ii) The approximately 56% increase in world petroleum consumption; and
(iii) The higher sulfur content in increasingly heavier feeds [2,4].

In addition, as newer, environmentally friendly technologies for energy production are developed, the demand for cleaner fuels will increase. Recent studies of fuel cells explore the possibility of using hydrocarbons as fuels, so that current technology can still be used in the production of combustibles [5]. Moreover, hydrocarbons have the advantage of having a higher power density than fuels such as alcohols. However, hydrocarbon should undergo a reformation in order to be used in fuel cells; this step may include the use of precious-metal catalysts. Since reforming catalysts and anode catalysts are very easily poisoned by the presence of sulfur, the sulfur should be reduced to levels even more stringent than that required to comply with the EPA Tier II regulations; therefore HDS catalysts are required to be even more effective.

* Corresponding authors.
E-mail addresses: camacho-bragado@mail.utexas.edu (G.A. Camacho-Bragado), yacaman@che.utexas.edu (M.J. Yacaman).

0021-9517/$ – see front matter
doi:10.1016/j.jcat.2005.06.009

Although much research has focused on developing this kind of catalyst, including the location of active sites, the reaction pathways, selectivity, and synthesis methods to maximize the number of active sites, there are still many aspects that remain to be understood [6–9].

A common approach to the maximization of the number of active sties is to decrease the particle size. In the particular case of nanosized TMS particles, there have been reported fullerene-like particles and nanotubes, which presented excellent lubrication properties [10–12]. More recently Olivas et al. [13] reported the simultaneous formation of NiS nanoparticles and nanorods of a WO_x core surrounded by a WS_2 thin shell.

Application of novel characterization techniques such as scanning tunneling microscopy (STM) and high-angle annular dark field (HAADF) to the study of catalysts [14–16] has led to significant advances in the understanding of the location of active sites and possible reaction mechanisms [17]. In particular, STM studies have confirmed that special metallic states exist at the edges of small MoS_2 clusters [15], meaning that when the particle size is restricted to a few nanometers, the electronic structure is distorted and different from that in the bulk material. Moreover, a recent work has reported a correlation between HDS activity and the presence of one-dimensional TMS structures in commercial catalysts [18].

Our aim in this paper was to find a synthetic approach for the formation of pseudo-one-dimensional structures of MoS_2, that is, structures that present nanometric sizes and very low stacking.

Thus we synthesized molybdenum sulfide catalysts by sulfidation of molybdenum oxide nanoribbons. The sulfidation of molybdenum oxides at high temperatures is known to produce fullerene-like species [19,20]. In an analogous way, it has been reported that the reaction between MoO_3 nanobelts at high temperatures in the presence of elemental S produces fullerene-like structures [20]; therefore we tried a different set of conditions to avoid the closure of the structure, that is, the fullerene formation. This was very desirable since the closed-cage structures would have only basal planes exposed to the reactants in the catalytic activity tests, and they are well known not to be active for HDS reactions [21,22].

It has also been proved that the sulfidation conditions affect the final morphology of the product [16,23], that is, the stacking and the edge termination can be varied with the synthesis conditions. Therefore, the catalytic behavior changes since it strongly depends on the type of surfaces present in the material [24,25]. We found that the conditions reported here favor the growth of a one-dimensional molybdenum sulfide phase without evidence of fullerene formation.

2. Experimental

A self-standing film of α-MoO_3 nanoribbons was prepared by a hydrothermal process. The procedure consisted of adding dropwise a 4 M solution of HCl to a saturated solution of sodium molybdate. The mixture is placed in a Teflon-lined autoclave and left at 423 K for 6 h (precursor of sample W) or 24 h (precursor of sample Y) [26]. Once the reaction time was completed, the product was filtered and dried.

Sections of these films were reacted with a stream of H_2S gas mixed with one of forming gas (90% inert gas/10% H_2) in a 9/1 volume ratio at 723 K for 1 h in order to produce the corresponding sulfide. Three different inert gases, nitrogen, argon, and neon, were used to study their influence on the morphology of the final product. The unreacted excess of H_2S was neutralized with a saturated solution of NaOH.

The resulting sulfides were placed on carbon tape and coated with Au–Pd. Their morphology was studied by scanning electron microscopy (SEM) in a Hitachi S-4500 field emission SEM operating at 5 kV and a Jeol JSM 7700F (Cs-corrected, 0.6-nm resolution) microscope operating at 2 kV.

For crystal structure identification we used a Phillips automated vertical scanning powder diffractometer. The spectra were obtained between 10 and 60 2θ degrees.

Transmission electron microscopy (TEM) and associated techniques such as energy-dispersive X-ray spectroscopy (EDS), nanobeam diffraction (NBD), selected area diffraction (SAD), high-resolution electron microscopy (HREM), dark-field imaging (DF), and high-angle annular dark field (HAADF) were applied to determine the subnanometer structure, chemical composition, and homogeneity of the sulfides. For TEM analysis, the samples were sonicated in isopropanol and deposited on lacey carbon on copper grids. TEM analysis was carried out in a JEOL 2010 F microscope equipped with a Schottky-type field emission gun, an ultra-high-resolution pole piece ($Cs = 0.5$ mm), and a scanning-transmission (STEM) unit with a high-angle annular dark-field detector (HAADF) operating at 200 kV. An Oxford spectrometer, attached to the 2010F, was used for EDS analysis.

HREM images were carried out with SimulaTEM, which performs fully dynamical calculations with the multislice method. The images were calculated at two defocus conditions with the parameters for the JEOL 2010 F (200 KV, $Cs = 0.5$ mm).

Specific surfaces areas were determined with a Nova 1000 series from Quantachrome by nitrogen adsorption at 77 K, with the BET method. Samples were degassed under vacuum at 523 K before nitrogen adsorption.

Reference catalysts were prepared by decomposition of ammonium thiomolybdate (ATM). One of them was sulfided ex situ in a tubular reactor with 15% volume H_2S/H_2 flow at 673 K for 4 h (heating rate 4 K/min) before catalytic testing; the other one was left to be sulfided in situ during the reaction. The decomposition of ATM precursor is a well-known reaction that occurs very fast, generating MoS_2, NH_3, and H_2S [27].

The HDS of dibenzothiophene (DBT) has been studied as a model reaction of HDS of petroleum feedstock. For

this work the HDS was carried out in a Parr Model 4520 high-pressure batch reactor. The catalyst was placed in the reactor (ex situ catalysts (1.0 g) or in situ catalysts, the appropriate amount of ATM to yield 1 g of MoS_2) along with the reaction mixture (5% volume of DBT in decaline), then pressurized to 3.4 MPa with hydrogen and heated to 623 K at a rate of 10 K/min under a constant agitation of 600 rpm. When the working temperature was reached, sampling for chromatographic analysis was performed to determine conversion versus time dependence; the reaction was run for 5 h. Reaction products were analyzed with an AutoSystem XL gas chromatograph (Perkin Elmer Instruments) with a 9-ft, 1/8-inch-diameter packed column containing OV-17 as the separating phase.

3. Results and discussion

We sulfidized sections of film of α-MoO_3 nanoribbons (Fig. 1A), keeping the H_2S/H_2 ratio constant at 90 and changing only the inert carrier gas. The sulfidation process produces metallic grey powders whose morphology differs from that one of the parent oxide. As can be seen in Figs. 1A and B, while the oxide particles are very homogeneous in size with smooth surfaces and a well-defined rectangular shape, the resulting sulfides are irregular, but still elongated particles (rods) with very rough surfaces. All three inert gases produced samples with very similar morphological features. Observation at higher magnification shows a series of platelets growing perpendicular to the long axis of the oxide (Figs. 1 C and D). It was observed by STEM that these bundles grow only within 10 to 30 nm from the surface. The chemical composition, as determined by EDS, showed only the presence of Mo, S, and O; no Na or Cl from the oxide precursors was found. Fig. 2A shows the average chemical composition; all of the analyzed data where within less than twice the standard deviation from the average value. The presence of O shows that at the temperature studied, the sulfidation reaction is not complete.

Fig. 2B shows the X-ray diffraction patterns of the two samples tested for catalytic activity. They were synthesized from oxides with different widths and thicknesses; the parent oxide nanoribbons of W were 124 nm wide, and those of sample Y were about 186 nm wide.

In both cases, X-ray diffraction showed the presence of two crystalline phases, molybdenum dioxide (Tugarinovite, JCPDS 78-1073) and molybdenum disulfide (Molybdenite-2H, JCPDS 65-0160) (Fig. 2B). The MoO_2 phase shows sharper and better-defined peaks than the MoS_2, suggesting that the sulfide is present as small crystallites that present an overall short-range order. This observation is in good agreement with the small sets of platelets observed by STEM. The electron diffraction patterns carried out on one of the long particles showed the presence of the two phases as well. Also observed was a set of spots that have been indexed as monoclinic MoO_2 superimposed to a set of rings, which correspond to MoS_2-2H (Fig. 2C). Conventional dark-field imaging (DF) of the rod-like particles allowed us to distinguish between the MoS_2-like phase growing on the surface and the MoO_2 matrix.

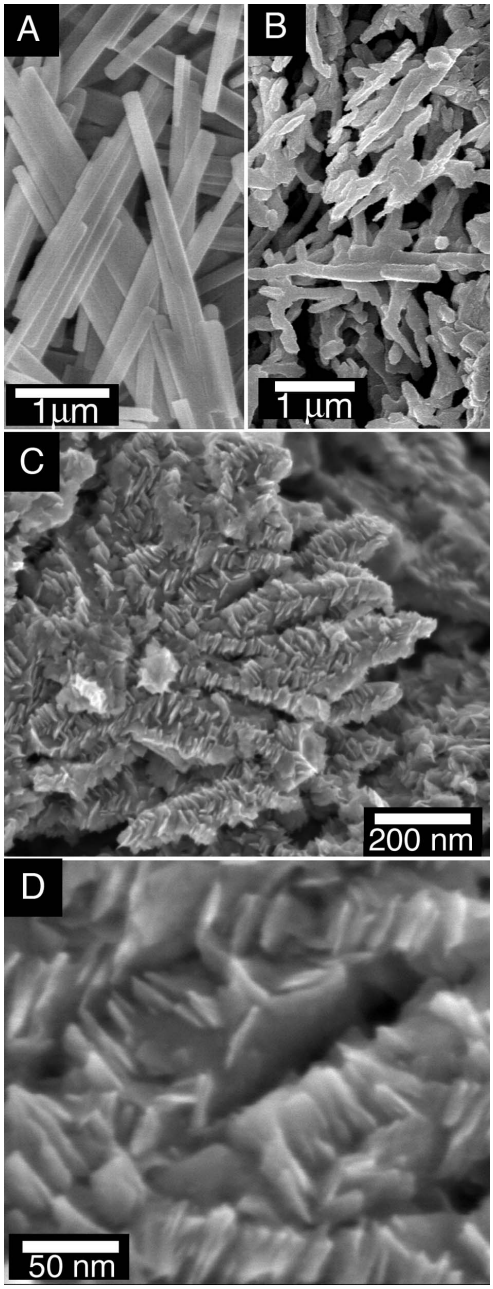

Fig. 1. (A) SEM image of the α-MoO_3 nanoribbons used as precursor for the sulfides. (B) After sulfidation these irregular elongated particles are observed. (C, D) Higher magnification of the sulfided sample, there can be seen a collection of platelets growing perpendicularly to the surface.

A more detailed study of the sulfide phases by HREM and HAADF showed two different terminations of the crystal. In some areas one can clearly see very thin sheets perpendicular to the long axis (Fig. 3A). HREM of those indicated that they correspond to MoS_2 basal planes (Fig. 3A, inset). In some other areas, one can observe needle-like terminations (Figs. 3B and C) that resemble bundles of nanowires.

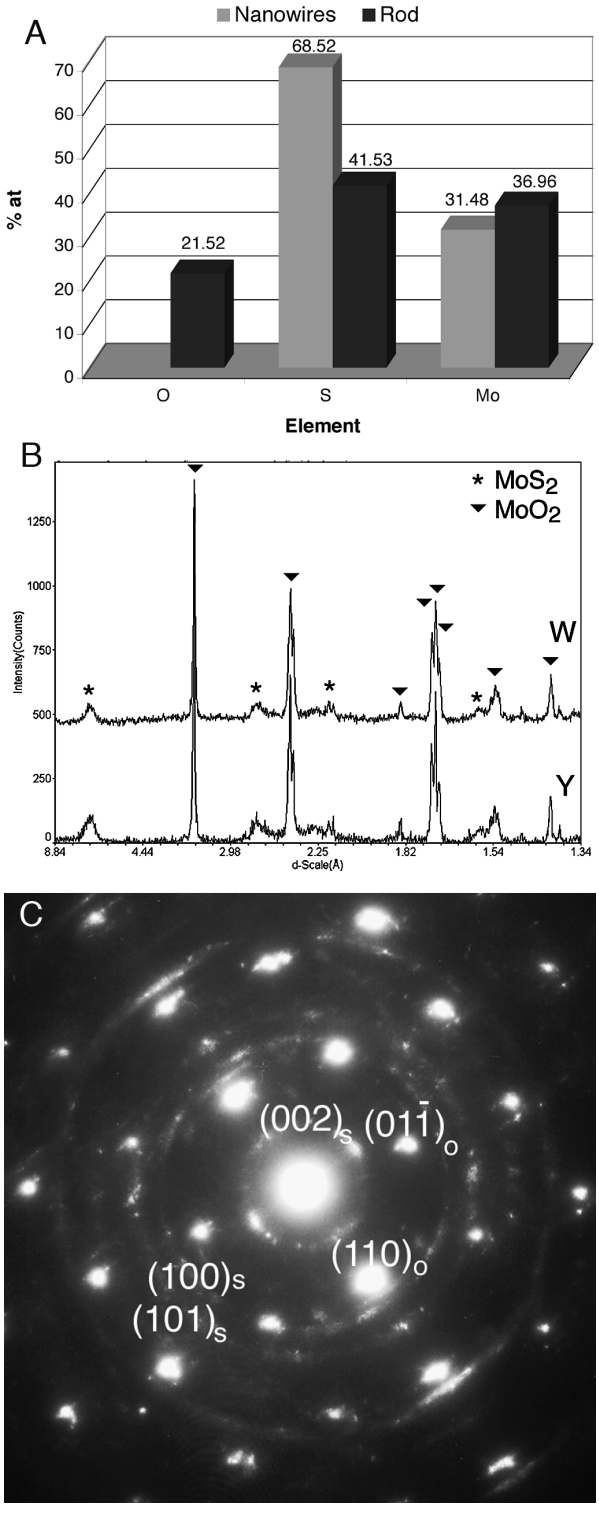

Fig. 2. (A) Elemental composition determined by EDS. (B) XRD pattern of the two samples tested for catalytic activity. (C) Electron diffraction pattern of one of the elongated particles, the spots are indexed as molybdenum dioxide, as indicated by a subindex 'o', and superimposed there can be seen the rings of the sulfide.

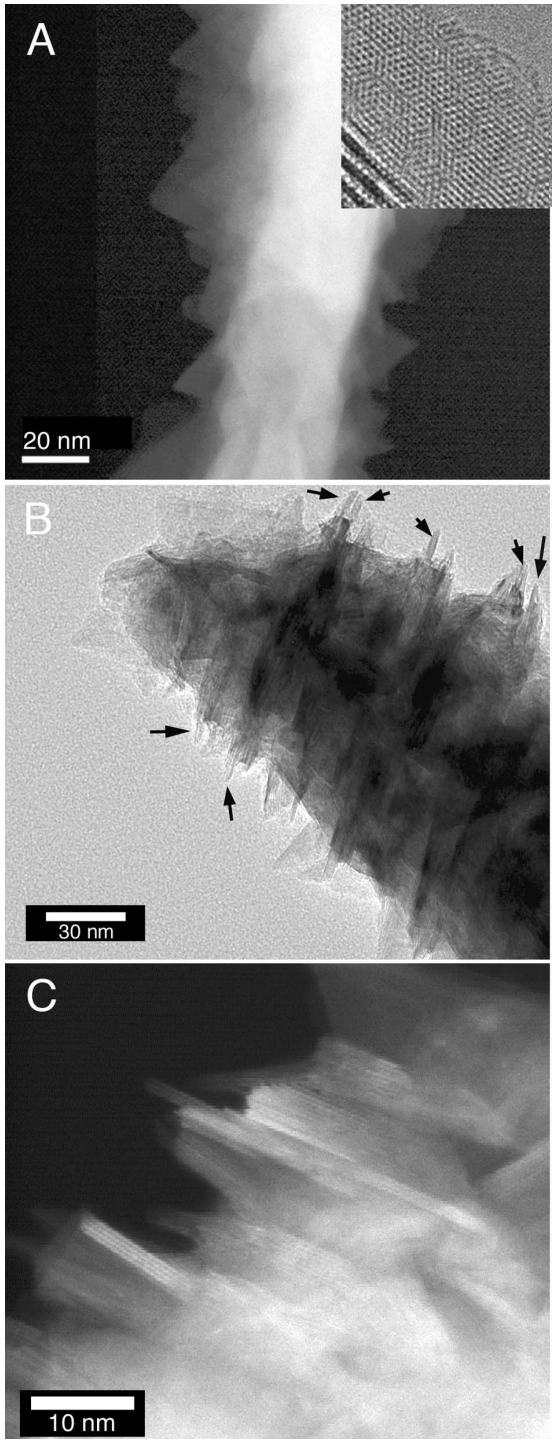

Fig. 3. (A) HREM image of one of the sheets showing the hexagonal array of (001) planes. (B) TEM of an area that presents multiple nanowire terminations (indicated by arrows) as well as some layers at the tip. (C) HAADF of the nanowires, the contrast is much stronger that the one of the hexagonal layers.

It is noticeable that oxygen was well localized at the rods and not detected in the nanowires. This observation, along with the DF results, supports the hypothesis that the core of the rod is MoO_2 crystal, and the outermost surface presents MoS_2 layers and bundles of nanowires of a MoS_2-like phase. The heterogeneous sulfidation can be explained to be due to the different reactivity along crystallographic directions in α-MoO_3 [28]. It is reported in the literature [26,28,29]

that MoO_3 nanobelts and nanoribbons grow preferentially along the [001] direction, which is the most reactive. Therefore, one would expect that the reduction-sulfidation would be more effective along this direction, whereas between the layers, in the [010] direction, mainly hydrogen will diffuse, allowing reduction to occur, forming MoO_2.

In several cases we have been able to observe a single or a pair of needles that grow well off the surface, allowing for a closer observation and to determine that they are actually single entities that can be regarded as nanowires with a thickness of half of the regular MoS_2-2H unit cell. Fig. 4 shows a HREM image of a bundle of nanowires where one is longer than the others in the bundle. The Fourier transform (FFT) of the single nanowire, shown in the inset, indicates that the wire grows along the [100] (Figs. 4A inset and B); an atomic resolved image of a nanowire shows the atoms in a hexagonal array (Fig. 4C), which implies that the nanowires have a MoS_2-like arrangement. EDS analysis performed in single nanowires and bundles of wires showed that they have a S/Mo ratio of about 2.3, whereas the S/Mo ratio was between 1.5 and 2 in the bigger rod-like particles. The rods also contain oxygen, which was expected, since tugarinovite (MoO_2) had been found by XRD and electron diffraction.

The nanowires seem to be very flexible, have a tendency to form bundles, and present a stronger contrast in HAADF than the regular MoS_2 layer, suggesting an important difference in the structure of the nanowires.

In order to understand the observed structures we built two models, shown in Figs. 5 and 6. The models were built from a single MoS_2 slab cut in such a way that it is limited by a $(10\bar{1}0)$ plane on one side and by a $(\bar{1}010)$ plane on the other. The edges can be saturated with sulfur in different ways to satisfy dangling bonds. In order to comply with the measured stoichiometry, two combinations were tested. In the first one (Fig. 5), the $(10\bar{1}0)$ edge was saturated with one S-atom per Mo-edge atom and the $(\bar{1}010)$ edge with two S-atoms per Mo-edge atom. For the second (Fig. 6), the $(10\bar{1}0)$ edge is saturated with two S per Mo atoms and the $(\bar{1}010)$ edge with one S per Mo-edge atom. Schweiger et al. [23] calculated the stability of these edges and showed the formation of S dimers at the so-called Mo edge $(10\bar{1}0)$ when it is saturated with two S atoms. The formation of disulfide ions at MoS_2 edges to complete coordination had already been predicted and is thought to be related to the catalytic activity of this compound [30,31].

The clusters chosen in such a way agree well with the dimensions measured from HREM and the growth direction determined from the FFT. HREM image simulations are shown in Figs. 5B, C and 6B, C. It was observed that at Scherzer defocus, the hexagonal array with an interatomic distance of 0.27 nm is reproduced (Figs. 5B and 6B). Furthermore, when a focal series is calculated, a contrast reversal is observed at a defocus of −15.5 nm; in these images (Figs. 5C and 6C) the contrast fully corresponds to that observed in the experimental images. Preliminary calculations of the electronic structure of the clusters shown in Figs. 5A and 6A indicate a soft metal behavior; a more detailed theoretical study will be reported elsewhere.

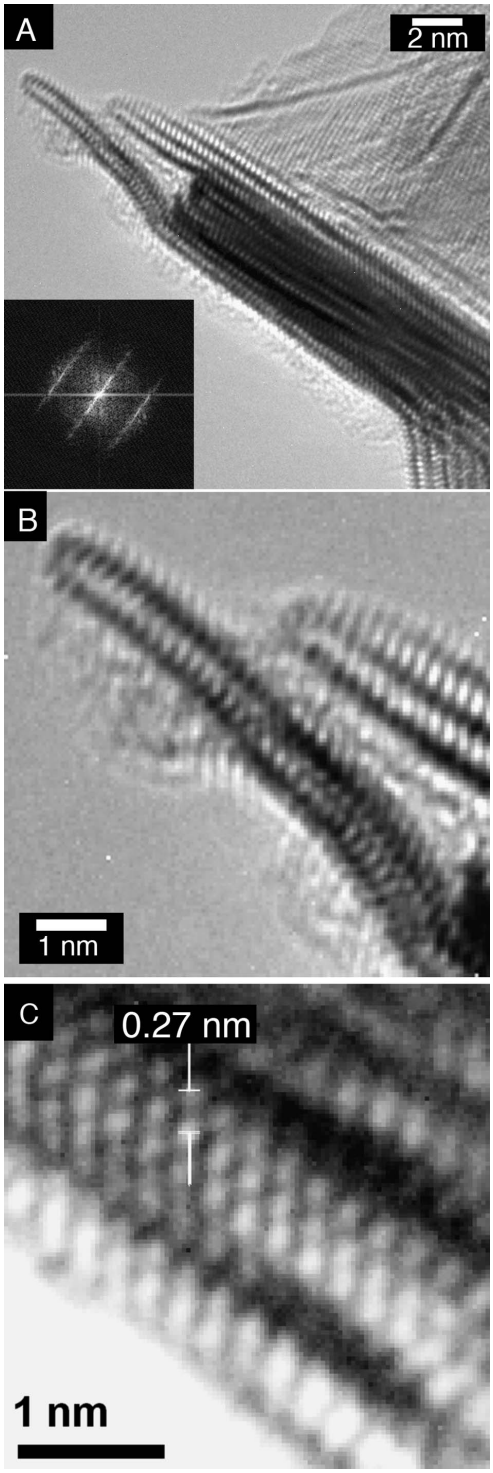

Fig. 4. (A) High resolution image of a bundle of nanowires. The Fourier transform shown in the inset confirms their one-dimensional character. (B) An amplification of the tip of one of the nanowires shown in A. (C) An atom resolved image of the lower part of one of the nanowires, it shows the hexagonal array presented along the body of the nanowire.

Bollinger et al. have calculated that one-dimensional metallic states form at the edges of single-layer MoS_2 clus-

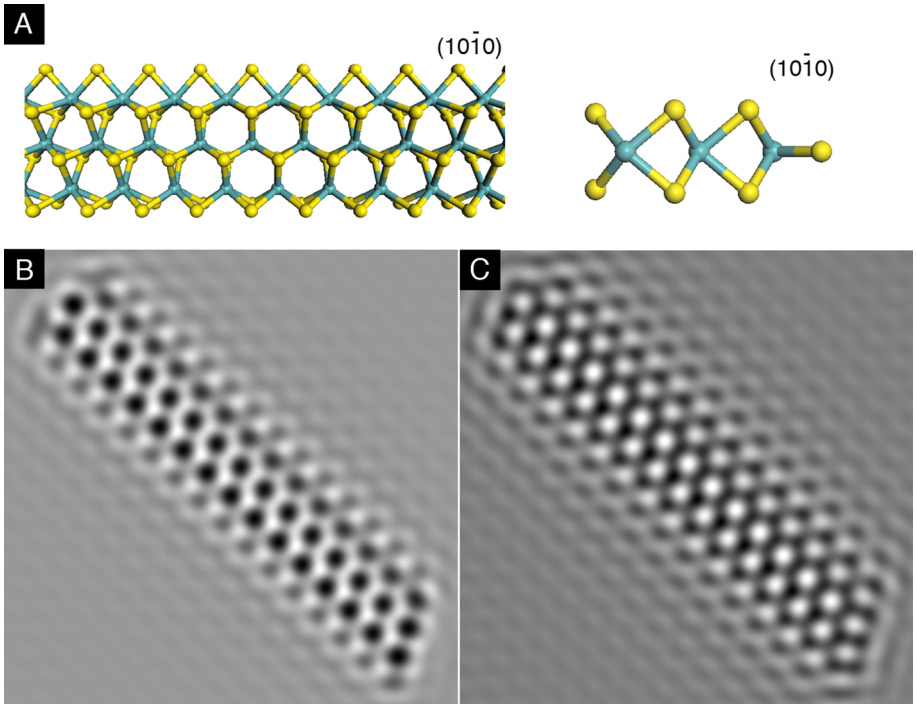

Fig. 5. (A) Side and top view of the model presenting 50% coverage on the Mo edge and 100% on the sulphur edge (blue spheres represent Mo atoms and yellow ones represent S). (B) HREM simulated image at Scherzer defocus (−34.5 nm), the hexagonal array is clearly observed. (C) HREM simulated image at a defocus value of −15.4 nm, the contrast shown at this defocus corresponds to the experimental image.

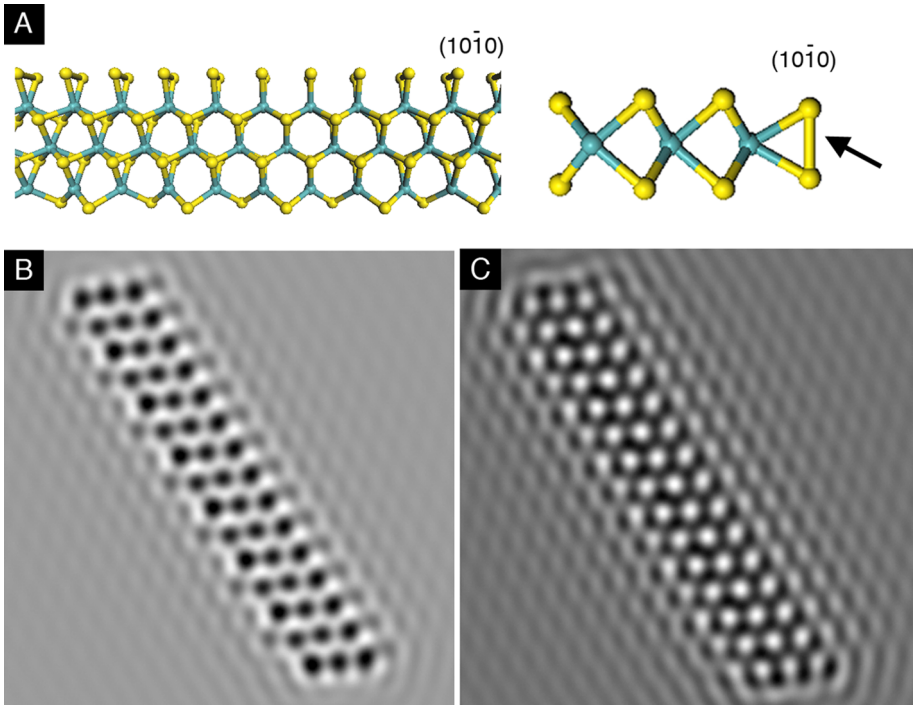

Fig. 6. (A) Side and top view of the model presenting 100% of sulphur coverage on the Mo edge and 50% on the sulphur edge. The location of the disulfide is indicated by an arrow (blue spheres represent Mo atoms and yellow ones represent S). (B) HREM simulated image at Scherzer defocus. (C) HREM simulated image at a defocus value of −15.4 nm, the contrast shown at this defocus corresponds more closely to the observed experimentally.

ters [15], which shows that if MoS_2 is confined to a size where only edges are present, both the geometric and the electronic configurations will be different from the bulk. It is then expected that the nanowires undergo a structural rearrangement, even though they would preserve a resemblance to the macroscopic crystal.

Table 1
Surface area calculated by the BET equation from nitrogen absorption at 77 K (before and after reaction), rate constants (k), and HYD/DDS ratios for HDS of DBT (3.4 MPa of hydrogen, 623 K)

Sample	Surface area before reaction (± 0.5) m^2/g	Surface area after reaction (± 0.5) m^2/g	Rate constant k ($\times 10^7$) ($mol\,s^{-1}\,g^{-1}$)	Selectivity HYD/DDS
W	14	10	3.7	1.5
Y	2	15	3.4	1.8
Ex situ reference	8		1.7	0.4
In situ reference	60		6.0	1.5

The formation of disulfide ions will produce a stronger contrast similar to the one produced by defects (the so-called Huang scattering [32,33]), resulting in a stronger intensity in the HAADF image due to local electron dechanneling effects.

The two sulfides tested for catalytic activity were morphologically very similar but presented different surface areas (Table 1). Compared with the surface of reference catalysts, sample W presents a typical value for this kind of catalyst, intermediate between the in situ and ex situ references, whereas sample Y presents a very low surface area, much lower than the lower limit set by the ex situ reference.

Interestingly, the two catalysts showed similar activities and selectivity for hydrogenation, in spite of the very different surface areas.

The surface area of catalysts after the HDS reaction test increased for the Y, whereas it decreased slightly for the W. Loss of surface area of catalysts during catalytic reaction is considered normal because of the formation of carbon deposits on the surface, particle sintering, or both; however, a surface area increase is not commonly observed. In this case the increase in surface area is attributed to disaggregation or separation of agglomerated nanoparticles due to stirring and high pressure inside the reactor. This could be a relevant aspect of nanostructured catalysts to be further studied. A similar case was observed in Ni/WS_2 nanostructured catalyst after the HDS of DBT reaction test [34].

Nevertheless, it has been observed for samples activated in situ; thus, in situ activation of tetraalkylammonium thiosalts was reported to provide catalysts with enhanced area and improved catalytic performance [35]. A similar effect is shown in Table 1 for reference samples, as in situ treatment generated a higher surface area than the ex situ one.

The same trend, but less marked, can also be observed for the Y sample, which presents a higher value after reaction. Surface-area results suggest that sample Y was not sufficiently sulfided before reaction.

The HDS of DBT was studied under conditions of 623 K and 3.4 MPa, which are close to those used in industrial applications. DBT was chosen because it is considered an appropriate compound for the investigation of activity and reaction mechanisms of proposed HDS catalysts, and it is widely used in the literature, which facilitates the comparison with data already reported.

The HDS of DBT yields two main products: biphenyl (BP) through the so-called direct desulfurization pathway (DDS) and phenylcyclohexane (PCH) through the hydrogenative pathway (HYD). Phenylcyclohexane is a secondary product along this pathway obtained by the C–S bond-breaking reaction from tetrahydrodibenzothiophene (THDBT), an intermediate product formed by hydrogenation of one of the aromatic rings of dibenzothiophene. Since these two pathways are parallel, the ratio between HYD and DDS can be approximated in terms of the experimental selectivity by means of the equation:

$$\frac{\mathrm{HYD}}{\mathrm{DDS}} = \frac{\mathrm{PCH}}{\mathrm{BP}}.$$

Nevertheless, changes between hydrogenating and hydrogenolysis (C–S bond breakage ability) functions can be better ascertained from a comparison of THDBT and BP, which are the primary products along the two parallel pathways. Indeed, THDBT is formed only by the hydrogenation of one of the aromatic rings of DBT, whereas BP is produced by direct C–S bond cleavage from DBT.

The experimental constant rate (pseudo-zero-order because the DBT concentration decreased linearly with time) is given in moles of DBT transformed by second in 1 g of catalyst, and it was calculated from the experimental slope of the plots of DBT concentration versus time according to the equation

$$\left[\mathrm{Slope(1/Hr)}\right] \times (\mathrm{Hr}/3600\ \mathrm{s}) \times (1\ \mathrm{mol}/1000\ \mathrm{mmol}) \times 34\ \mathrm{mmol} \times (1/g_{\mathrm{cat}}),$$

where 34 mmol is the initial concentration of DBT.

The pseudo-zero-order rate constant values (k), calculated from the slope of the experimental data on DBT conversion versus time, are listed in Table 1. The ex situ reference sample presents a rate constant of 1.7×10^{-7} $mol\,s^{-1}\,g^{-1}$, which is considered to be a standard value for typical unsupported MoS_2. The in situ MoS_2 reference shows an improvement of activity with a rate constant of 6.0×10^{-7} $mol\,s^{-1}\,g^{-1}$. Such an effect can be attributed primarily to surface-area improvement (from 8 to 60 $m^2\,g^{-1}$), provoking an increase in contact area between reactive and catalyst surfaces. The W and Y catalysts have similar catalytic activities (3.4–3.7×10^{-7} $mol\,s^{-1}\,g^{-1}$. They are more efficient catalysts than ex situ MoS_2 but less than in situ. The enhancement of activity observed in sulfide–oxide catalysts with respect to the ex situ reference is more related to the morphology change of particles (nanowires and single layers) than the surface-area improvement, which is modest. The morphology changes expose catalytically active sites, especially those located at the borders of the nanowires, increasing the activity.

The reference ex situ catalyst showed a selectivity ratio of 0.4, which is a typical value for MoS_2 or $Co–Mo/Al_2O_3$ industrial catalysts favoring the DDS reaction pathway [36].

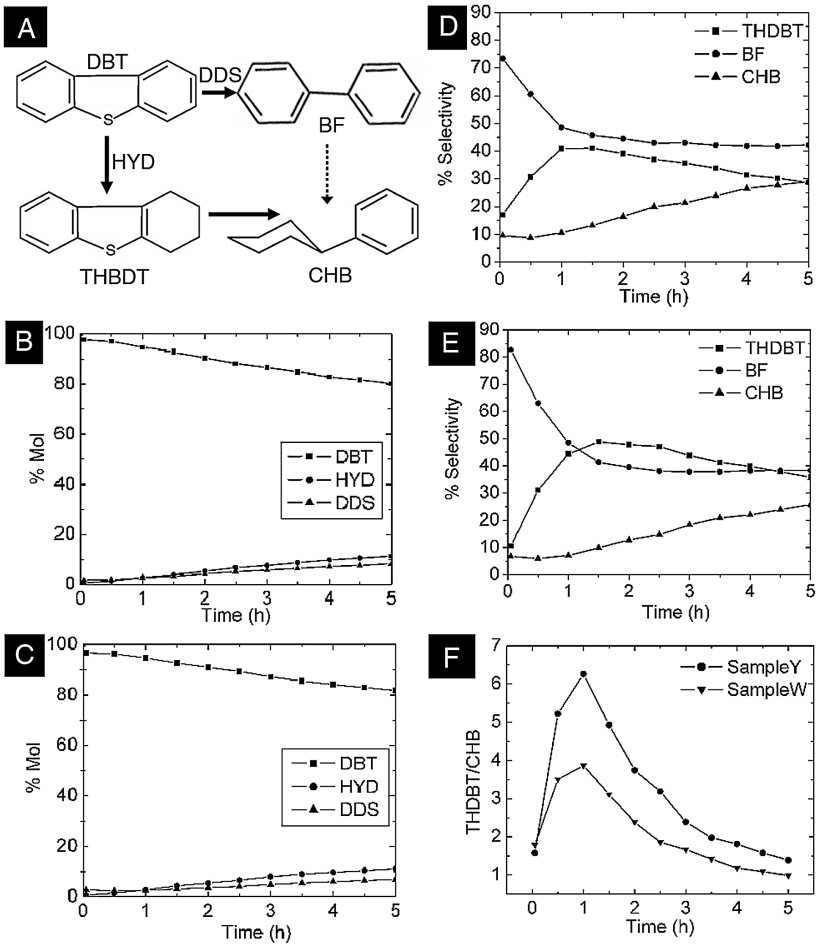

Fig. 7. (A) Scheme of the HDS of DBT pathways. (B, C) Catalytic activity plots for the HDS of DBT (samples W and Y, respectively). (D, E) Molar selectivity plots of samples Y and W. (F) Hydrogenation products ratio, showing the continuous production of the intermediate hydrogenation product (THDBT).

The DDS pathway is also known to occur preferentially in Co–Mo/Al_2O_3 industrial catalysts [37,38]. Conversely, the in situ reference catalyst presents a selectivity ratio of 1.5, indicating that hydrogenation of the aromatic ring occurred more extensively. High selectivity for hydrogenation was also observed in sulfide–oxide catalysts (1.54 for W and 1.84 for Y).

Fig. 7 shows the distribution of the reaction products of HDS of DBT. The final hydrogenation (HYD) products were cyclohexylbenzene (CHB) and tetrahydrodibenzothiophene (THDBT), and biphenyl (BF) of direct desulfurization (DDS). No other products such as benzene or bicyclohexyl were detected after 5 h of reaction. As mentioned in Table 1 and according to the literature [39,40], the HDS occurred mainly through the hydrogenation pathway (Fig. 7A).

It can be seen from the product distribution (Figs. 7B and C) that the DDS product (biphenyl) increases almost linearly during the 5 h that the catalysts were tested. The production of CHB also steadily increased as expected, but the THDBT showed an unusual behavior. It was noticed that whereas the THDBT/CHB ratio for the MoS_2 microcrystals (after [41]) reached a maximum briefly after 1 h and then abruptly decreased within the next 30 min, for our samples the maximum is reached in a shorter time, but then it decreases smoothly to a value close to 0.8, which is higher than the minimum for MoS_2 microcrystals.

This result indicates that THBDT continues to be produced, but there may not be enough sites for the final C–S bond cleavage to occur, and therefore not all of the THDBT can be converted to CHB.

We can explain the activity of this material in terms of the reaction pathway proposed by Lauritsen et al., based on their STM and spectroscopy results [42]. Traditionally, it was believed that the HDS reactions occur at sulfur vacancies on the MoS_2, but in situ STM observations of the interaction between MoS_2 clusters and thiophene indicate activity at the metallic edges, which seem to be terminated by sulfur dimers. The presence of sulfur dimers was also discussed by Goodenough as a way to complete the coordination of the molybdenum atoms lying on the surface of molybdenum sulfide [30].

In accordance with such a mechanism, we propose that the DBT molecules are physisorbed to the MoS_2 nanowires, which present an excess of sulfur; and partial hydrogenation occurs at that site, forming THDBT. Later on, the THDBT molecule must be desorbed from this site and be adsorbed

in a site able to accept S, for the C–S bond to be broken. The single MoS_2 layers may play the role of a drain for this excess sulfur. Those sites may also be where DDS occurs; therefore the formation of BP and that of CHB are competitive, and hence not all of the THDBT can be consumed under the conditions tested.

4. Conclusions

We have shown the synthesis of a nanostructured self-supported catalyst containing MoS_{2+x} nanowires. It was detected that a strong sulfiding atmosphere stabilized the growth of bundles of MoS_{2+x} nanowires, which have a structure that deviates from the bulk, allowing for the formation of S dimers at the edges. It was found that the edges must present a higher S concentration than the bulk to stabilize the nanowire structure.

The ability of S-saturated edges to donate and accept electrons is believed to enhance catalytic activity [30]. However, they do not seem to be the most favorable sites for the final C–S bond cleavage, since the reaction intermediate (THDBT) was not totally consumed. Nevertheless, we have shown that the selectivity of molybdenum sulfide catalysts can be tailored by the creation of new structures at the nanoscale that differ from the bulk in structure and reactivity.

Acknowledgments

The authors thank Dr. Jose Reyes for fruitful discussions. We also appreciate the technical assistance of Carlos Ornelas from CIMAV and G. Alonso. JEOL, Ltd. is acknowledged for providing access to the high-resolution SEM. HREM images were simulated with the SimulaTEM program. Financial support was provided by the AMRC SEMATECH fund, DGAPA, through grant IN119602-3 and project PAPIIT IN119602-3. G.A.C.B. is grateful for the fellowship granted by CONACyT.

References

[1] E.E. Donath, in: J.R. Anderson, M. Boudart (Eds.), Catalysis, Springer, Berlin, 1982, p. 1.
[2] C. Song, Catal. Today 86 (2003) 211.
[3] EPA, control of air pollution from new motor vehicles amendment to the tier-2/gasoline sulfur regulations, US Environmental Protection Agency, April 13, 2001, http://www.epa.gov/fedrgstr/EPA-AIR/2001/April/Day-13/a8927.htm.
[4] EIA/AER, Annual Energy Review 2001, Energy Information Administration, US Department of Energy, Washington, DC, 2002.
[5] C. Song, Catal. Today 77 (2002) 17.
[6] G. Hagenbach, B. Delmon, Comptes Rend. Seanc. Acad. Sci. C: Sci. Chim. 273 (1971) 1489.
[7] R.R. Chianelli, Catal. Rev. Sci. Eng. 26 (1984) 361.
[8] R. Prins, V.H.J. Debeer, G.A. Somorjai, Catal. Rev. Sci. Eng. 31 (1989) 1.
[9] B.G. Silbernagel, T.A. Pecoraro, R.R. Chianelli, J. Catal. 78 (1982) 380.
[10] L. Rapoport, Y. Bilik, Y. Feldman, M. Homyonfer, S.R. Cohen, R. Tenne, Nature 387 (1997) 791.
[11] R. Tenne, Colloids Surf. 208 (2002) 83.
[12] R. Tenne, L. Margulis, M. Genut, G. Hodes, Nature 360 (1992) 444.
[13] A. Olivas, A. Camacho, M.J. Yacaman, S. Fuentes, J. Mater. Res. 19 (2004) 2176.
[14] S. Helveg, J.V. Lauritsen, E. Laegsgaard, I. Stensgaard, J.K. Norskov, B.S. Clausen, H. Topsoe, F. Besenbacher, Phys. Rev. Lett. 84 (2000) 951.
[15] M.V. Bollinger, J.V. Lauritsen, K.W. Jacobsen, J.K. Norskov, S. Helveg, F. Besenbacher, Phys. Rev. Lett. 87 (2001) 196803.
[16] J.V. Lauritsen, M.V. Bollinger, E. Laegsgaard, K.W. Jacobsen, J.K. Norskov, B.S. Clausen, H. Topsoe, F. Besenbacher, J. Catal. 221 (2004) 510.
[17] H. Topsoe, B.S. Clausen, F.E. Massoth, Hydrotreating Catalysis, Science and Technology, Springer Verlag, Berlin, 1996.
[18] M. Perez De la Rosa, S. Texier, G. Berhault, A. Camacho, M. José Yácaman, A. Mehta, S. Fuentes, J.A. Montoya, F. Murrieta, R.R. Chianelli, J. Catal. 225 (2004) 288.
[19] Y. Feldman, E. Wasserman, D.A. Srolovitz, R. Tenne, Science 267 (1995) 222.
[20] X.L. Li, Y.D. Li, Chem. Europ. J. 9 (2003) 2726.
[21] S. Kasztelan, Langmuir 6 (1990) 590.
[22] M. Salmeron, G.A. Somorjai, A. Wold, R. Chianelli, K.S. Liang, Chem. Phys. Lett. 90 (1982) 105.
[23] H. Schweiger, P. Raybaud, G. Kresse, H. Toulhoat, J. Catal. 207 (2002) 76.
[24] L.S. Byskov, J.K. Norskov, B.S. Clausen, H. Topsoe, J. Catal. 187 (1999) 109.
[25] L.S. Byskov, J.K. Norskov, B.S. Clausen, H. Topsoe, Catal. Lett. 64 (2000) 95.
[26] G.A. Camacho-Bragado, J. Reyes-Gasga, M. José Yácaman, Appl. Phys. A, submitted for publication.
[27] T.P. Prasad, E. Diemann, A. Muller, J. Inorg. Nucl. Chem. 35 (1973) 1895.
[28] X.L. Li, J.-F. Liu, Y.D. Li, Appl. Phys. Lett. 81 (2002) 4832.
[29] P. Delporte, F. Meunier, C. Pham-Huu, P. Vennegues, M.J. Ledoux, J. Guille, Catal. Today 23 (1995) 251.
[30] J.B. Goodenough, in: H.F. Barry, P. Mitchell (Eds.), 4th International Conference on the Chemistry and Uses of Molybdenum, Climax Molybdenum, Ann Arbor, MI, 1982, p. 1.
[31] L.S. Byskov, B. Hammer, J.K. Norskov, B.S. Clausen, H. Topsoe, Catal. Lett. 47 (1997) 177.
[32] Z.-L. Wang, Ultramicroscopy 53 (1994) 73.
[33] Z.-L. Wang, Acta Crystallogr. A 51 (1995) 569.
[34] A. Olivas, M.J. Yacaman, E. Flores, G. Alonso, S. Fuentes, in: American Catalysis Society Meeting, Philadelphia, 2005.
[35] G. Alonso, M. Del Valle, J. Cruz, V. Petranovskii, A. Licea-Claverie, S. Fuentes, Catal. Today 43 (1998) 117.
[36] G. Alonso, M. Del Valle, J. Cruz, A. Licea-Claverie, V. Petranovskii, S. Fuentes, Catal. Lett. 52 (1998) 55.
[37] M. Nagai, T. Kobe, J. Japan Petroleum Inst. 23 (1980) 82.
[38] M.L. Vrinat, Appl. Catal. A 6 (1983) 137.
[39] M. Egorova, R. Prins, J. Catal. 225 (2004) 417.
[40] M. Kouzu, K. Uchida, Y. Kurili, F. Ikazaki, Appl. Catal. A 276 (2004) 241.
[41] M. Daage, R.R. Chianelli, J. Catal. 149 (1994) 414.
[42] J.V. Lauritsen, M. Nyberg, J.K. Norskov, B.S. Clausen, H. Topsoe, E. Laegsgaard, F. Besenbacher, J. Catal. 224 (2004) 94.